In Vitro and In Vivo Imaging of Ultra–High-Molecular-Weight Polyethylene Orbital Implants

Marek Olszycki, PhD[1]/Marcin Kozakiewicz[2]/Marcin Elgalal, PhD[1]/
Agata Majos[3]/Ludomir Stefanczyk[3]

The aim of this study is to compare magnetic resonance imaging (MRI) with computed tomography (CT) for visualization of an orbital alloplastic prosthesis made of ultra–high-molecular-weight polyethylene (UHMW-PE) both in vitro and in vivo. A study of 15 test implants from UHMW-PE visualized in vitro in CT and MRI and an in vivo visualization in a patient who suffered from orbital injury and underwent reconstructive surgery is presented. The postsurgery MRI showed the UHMW-PE material clearly, with no significant artifacts. The surrounding tissues could be satisfactorily evaluated. The CT scans did not present the graft material. Both techniques were sufficient tools for in vitro evaluation of the shape and measurement of the prosthesis.
Int J Oral Maxillofac Implants 2015;30:e24–e29. doi: 10.11607/jomi.3790

Key words: *alloplastic prosthesis, computed tomography, magnetic resonance imaging, orbital injury, ultra–high-molecular-weight polyethylene*

Ultra–high-molecular-weight polyethylene (UHMW-PE) is a fairly novel material for maxillofacial surgery.[1] Such patient-specific implants are durable, can be used to reconstruct even very thin walls, do not exhibit the high degree of morbidity characteristic of autogenous bone grafts, and result in restoration of visual function.

The first objective of this survey was to evaluate and compare the ability of a standard ophthalmic magnetic resonance imaging (MRI) and computed tomography (CT) to visualize this new alloplastic prosthetic material, both in vitro and implanted within the orbital wall in a posttraumatic patient. The second objective was to assess possible artifacts caused by the alloplastic material.

Fifteen test implants were prepared for this study from medical UHMW-PE (Fig 1).[1] The test implant was designed and manufactured in a computer-assisted process. One base of the test implant was flat, and at its center the dome was measured for concavity depth. The goals of the design of the shape were easy measurements of the dimensions and simple detection of deformations. The mass of the detail was approximately 0.3 g, and the volume was 0.3 cm^3. Measurements of each test implant were made three times each, and the average was calculated.

Each implant was examined in vitro with multislice CT (MCT) and MRI after being placed inside syringes filled with two different fatty materials (pure cosmetic petroleum jelly and vegetable oil), which could imitate, to some extent, orbital fat (Figs 2a and 2b). Additionally, the implants were placed inside a muscle-fat mass (pork sausage) to better imitate the environment of the orbit (Figs 2c and 2d).

This investigation was undertaken on an MCT scanner (Light Speed VCT, GE Healthcare; equipped with AW Volume Share 5 adv 4.6 workstation). This scanner simultaneously acquires 64 slices, 0.625 mm each, over a 40-mm-thick region.

In every MCT and MRI series, a standard ophthalmic protocol of acquisition was used and was the same as the protocol used for the in vivo examination, which is described in the following. The measurements of the implant's dimensions in MCT and MRI were used exclusively on the basis of the series achieved in vegetable oil, because these were the only sufficiently readable images. In addition, three-dimensional (3D) MCT reconstructions of the implant submerged in the oil were produced (Fig 3).

[1]Medical University of Lodz, Department of Radiology, Lodz, Poland.
[2]Professor, Medical University of Lodz, Department of Maxillofacial Surgery, Lodz, Poland.
[3]Professor, Medical University of Lodz, Department of Radiology, Lodz, Poland.

Correspondence to: Dr Marek Olszycki, Medical University of Lodz, Department of Radiology, Kopcińskiego 22, 90-153 Lodz, Poland. Fax: +48-678-67-34.
Email: marek.olszycki@umed.lodz.pl

Fig 1 Test implant made of medical UHMW-PE. *(a)* Series of prefabricated implants. *(b)* Final test implant.

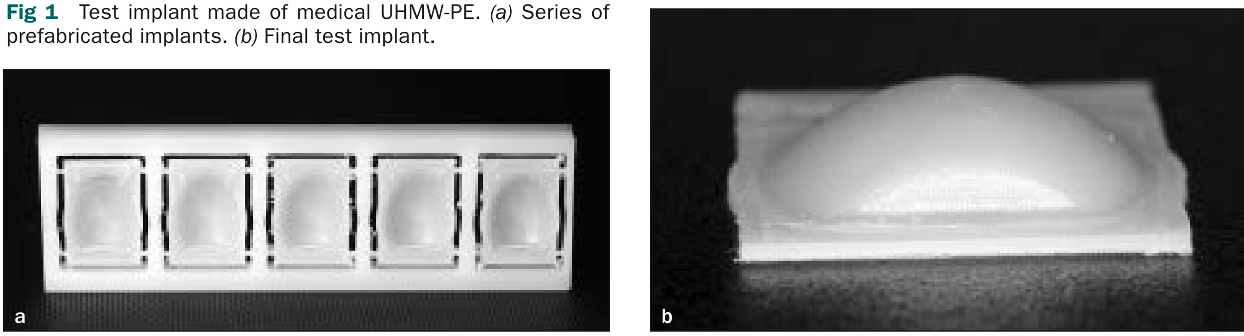

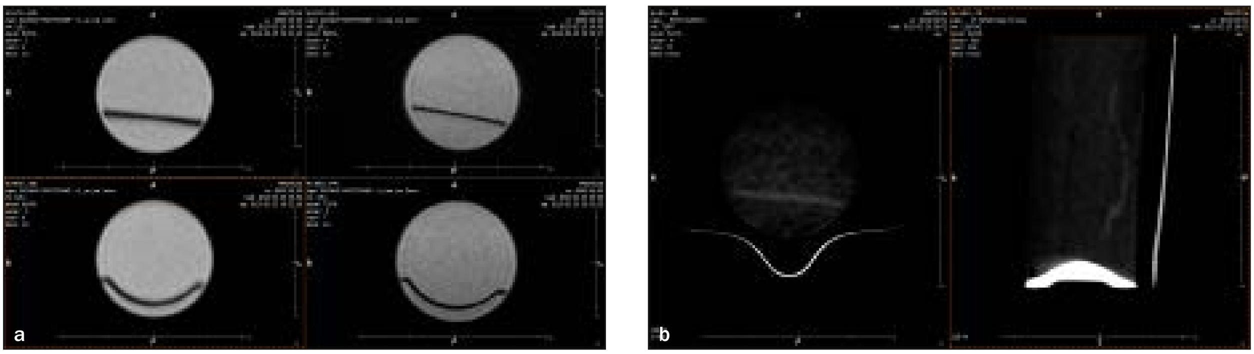

Figs 2a and 2b Test implant in vegetable oil; (*a*) T1-weighted MRI; (*b*) MCT.

Figs 2c and 2d Test implant in the muscle-fat mass in (*c*) MCT and (*d*) T1-weighted MRI.

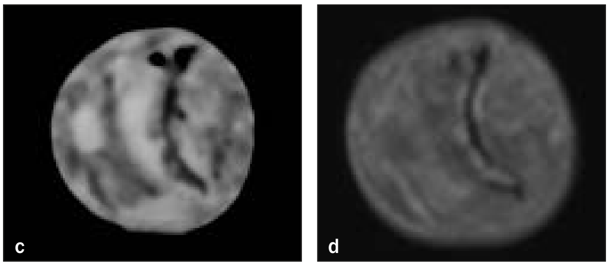

Statistical analyses of the in vitro measurements were performed in Statgraphics Centurion XVI. Mean values of the measurements were compared by *t* test (ie, average as normal distribution) or by the sign test (for samples where no normal distribution was observed). The significance level was established at $P < .05$.

Moreover, a patient with a comminuted fracture of the orbital walls who underwent extensive reconstructive surgery was studied. The affected globe and the malar region were supported with an especially large amount of alloplastic material (UHMW-PE), and the maxillary sinus was separated from the orbit. Before surgery, an MCT examination was performed to assess the orbital morphology (Fig 4).

On the basis of the CT, virtual models of both orbits were prepared in the mode described previously.[2,3] The injured orbit was enlarged significantly as a result of dislocation of its walls. The 3D model of the facial skeleton was symmetrically divided into two parts. This resulted in two models (left and right orbit). The uninjured orbit was then superimposed onto the contralateral, affected side. As a result, two surfaces were created. The outer surface (taken from the injured orbit) was used to design the outer surface of the implant, and the inner (taken from the intact orbit) was used for the inner surface. By combining both of these surfaces, the authors could determine the unique shape and thickness of the UHMW-PE implant

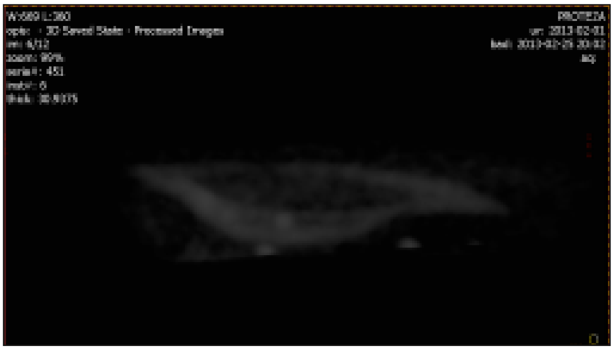

Fig 3 The 3D MCT reconstruction of the implant submerged in oil.

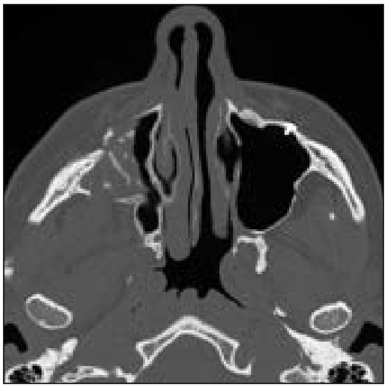

Fig 4 CT in axial plane shows a well-visualized fragmented bone defect in the right orbital floor.

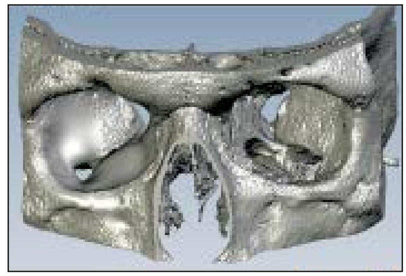

Fig 5a The computer-aided design of the clinical implant. After bone segmentation of the CT data, the virtual model with prepared surfaces was created in the right orbit before mirroring it on the left side to fix the bone defect in the orbital floor.

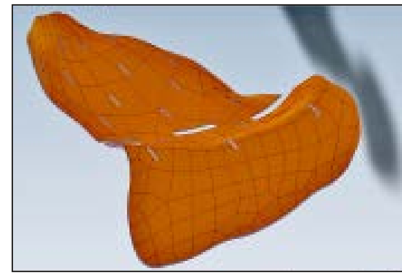

Fig 5b Final design of the UHMW-PE implant for reconstruction of the left orbital wall. Note the inclusion of foramina in the implant for eventual lowering of blood pressure in the retrobulbal space.

Table 1 Survey Results

	Image quality							
	T1 MRI images				T2 MRI images			
Structure	0	1	2	3	0	1	2	3
Orbital wall		x				x		
Muscles				x				x
Fat				x				x
Optic nerve				x			x	
Graft				x			x	
Artifacts	x					x		

The quality of the images was graded from 0 = worst to 3 = best.

that would allow for accurate reconstruction of the orbit. These data were transferred to computer software, and a numeric code for a five-axis milling machine was generated (Fig 5). The manufactured implant was sterilized in gas plasma and used to reconstruct the orbital walls.

After surgery, the affected orbit was visualized on a 1.5-T scanner (Siemens Magnetom) using a standard ophthalmic MRI protocol: T1-weighted spin-echo (repetition time, 2,200 ms; echo time, 80 ms) and T2-weighted fat-suppressed fast spin-echo (repetition time 1,560 ms; echo time, 50 ms) with a 256 × 256 matrix and a 3-mm slice thickness in the axial, frontal, and sagittal planes. The second visualization was MCT, done as in the preoperative manner.

The obtained images were analyzed and graded (0 to 3) according to the quality of visualization of the postsurgical orbital morphology and the implanted polymer. The depictions of the orbital walls, muscles, optic nerve, orbital fat, and the UHMW-PE prosthesis were all evaluated (Table 1).

The next focus of the evaluation was to assess image artifacts caused by the alloplastic material within the surrounding structures. The dimensions of the UHMW-PE implant image were distorted with respect to its actual size. The longest distance measure (length of the implant) was presented relatively accurately. There was only slight undermeasurement of the implant's length in the MRI examination (test statistic = 3.9442, $P < .005$). The width of the implant was significantly higher in MCT (test statistic = 3.0984, $P < .005$) and MRI (test statistic = –5.4637, $P < .0001$), and both imaging techniques overestimated this dimension equally. CT returned inaccuracies regarding the implant's thickness. The thickness of the implant was falsely increased relative to the actual measurement (test statistic = –9.3516, $P < .0001$) and relative to the MRI measurement (test statistic = 5.6636, $P < .0001$). MRI measurements of thickness and concavity depth were precise. In MCT examination of concavity depth, in contrast to the thickness measurement, the size observed was smaller than the actual measurement (test statistic = 3.4256, $P < .005$).

Analysis of the linear regression revealed that the longest actual distance measurements of the implant (length and width) had a moderately strong relationship to the shortest distance measurements (thickness of the implant) (length: F = 11.10, $P < .001$, correlation coefficient = –0.68, R-squared = 46%; width: F = 21.23, $P < .0001$, correlation coefficient = 0.79, R-squared = 62%). There was no such relationship in the measurements of the test implant obtained via MCT or MRI. The same was seen for longer distance measurements (length and width) in relation to another short distance measurement, concavity depth: length: F = 11.65, $P < .005$, correlation coefficient = 0.69, R-squared = 47%; width: F = 23.58, $P < .0005$,

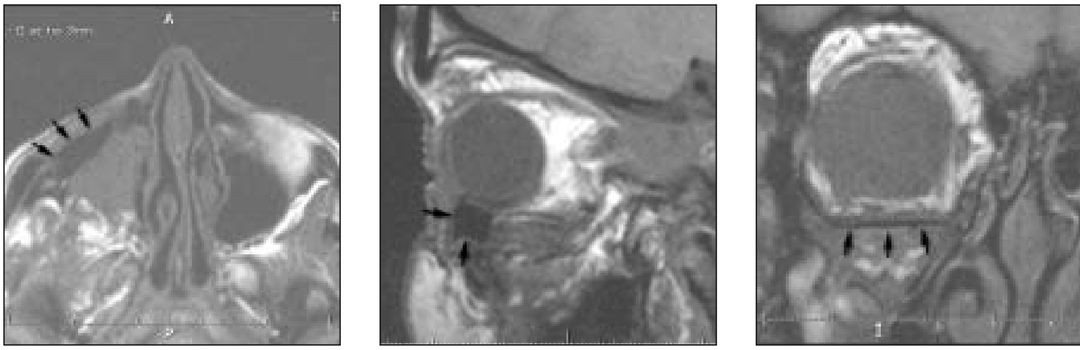

Fig 6 Linear regression analyses. There is a moderately strong relationship (*P* < .0005) between the true implant width and the true implant concavity depth, but when these measurements were performed on CT or MR images, this relationship disappeared.

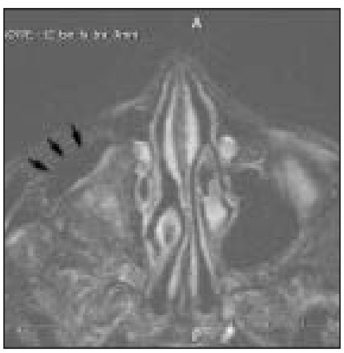

Fig 7 T1-weighted MRIs in (*left*) axial, (*center*) sagittal, and (*right*) frontal planes. Bone frame of the right orbit is surgically reconstructed. The UHMW-PE material is clearly visible (*arrows*).

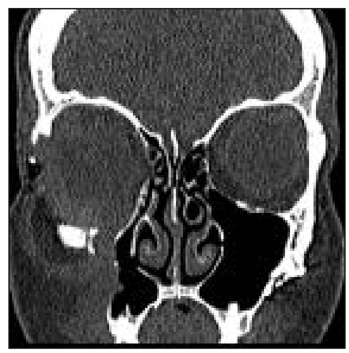

Fig 8 T2-weighted MRI in axial plane. UHMW-PE material is also quite visible.

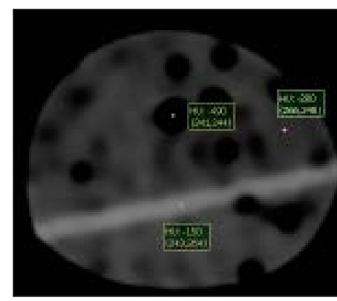

Fig 9 Postsurgical CT in coronal plane. The UHMW-PE material is not visible.

correlation coefficient = 0.80, R-squared = 64%. The detailed results are presented in Fig 6.

The postoperative MRIs of all standard ophthalmic sequences showed the UHMW-PE material quite clearly with no significant artifacts. In both T1- and T2-weighted images, the implant presented as a no-signal-intensity area and was quite smoothly delineated. The surrounding tissues could be also satisfactorily evaluated (Figs 7 and 8).

MCT did not present the implant in an acceptable manner. Only a slight change in the density was evident in the known location of the implant (Fig 9). The detailed results of the survey analysis are presented in Table 2.

Table 2 Measurement of Ultra-High Molecular Weight Polyethylene Test Implants in CT and MR

	Real test implant	CT	MR
Length	34.93 ± 1.02^{MR}	34.78 ± 1.18	34.31 ± 1.06^{R}
Width	22.75 ± 0.47$^{CT, MR}$	^{a}23.64 ± 0.79^{R}	23.51 ± 0.86^{R}
Thickness	0.82 ± 0.17^{CT}	1.25 ± 0.22$^{R, MR}$	0.89 ± 0.13^{CT}
Concavity depth	5.71 ± 0.29^{CT}	5.51 ± 0.33^{R}	5.60 ± 0.37

Superscripts indicate statistically significant difference: CT = computerized tomography; MR = magnetic resonance imaging; R = real test implant.
[a]No normal distribution was observed.

Titanium and polypropylene, along with bioactive glasses, glass-ceramics, polytetrafluoroethylene, silicone, and polyethylene, are alloplastic materials widely used for the repair of bone defects within the orbit.[4–9] UHMW-PE had not yet been assessed in this context within the orbit or face and, to the authors' knowledge, has not been previously described in the literature. UHMW-PE exhibits a combination of excellent properties: outstanding abrasion resistance, superior impact resistance, nonsticking

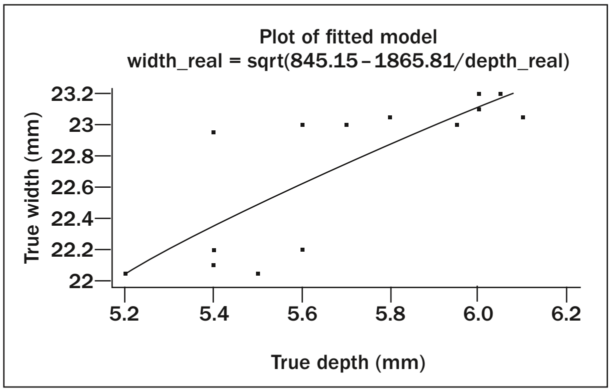

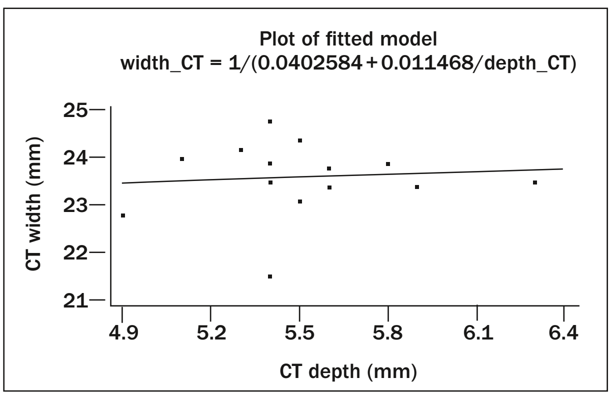

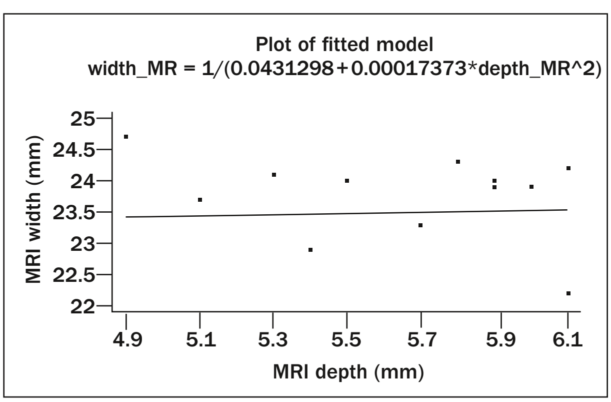

Fig 10 MCT image of implant in petroleum jelly, with some air collection. Note the density of each substance: UHMW-PE = –150 HU; petroleum jelly = –200 HU; air = –490 HU.

and self-lubricating features, and excellent mechanical properties. It is a polymer of extremely high viscosity that is produced in the form of powder and has an average particle diameter ranging from 100 to 200 μm. Because of its viscosity, it generally cannot be processed by methods commonly used for ordinary thermoplastics. Compression molding and ram extrusion are used to generate the high pressure needed to fuse UHMW-PE particles together, and then the material is typically formed into stock shapes or solid blocks, as necessary for milling (Ticona Engineering Polymers).

MCT and MRI are the principal radiologic methods used to monitor maxillofacial patients,[5,10,11] which is why the authors decided to test their ability to visualize these new implants, both in vitro and in vivo. Among the three tested fatty media—pure cosmetic petroleum jelly, vegetable oil, and pork sausage—the images achieved in oil were the only ones that could be used for the measurements because of the lack of artifacts. Inside the petroleum jelly and the sausage, the air collections along the surfaces and rims of the implants significantly hindered delineation of the graft (Fig 10). Because of these artifacts, it was decided to measure the implants exclusively on the basis of the images captured in oil. However, the small air bubbles within the prosthesis might imitate the real orbital environment after the surgery. The 3D MCT reconstructions of the implant submerged in oil were not very convincing and difficult to produce (because of the very narrow HU window), but the shape was recognizable (Fig 3).

According to the statistical analysis of the in vitro measurements, on MCT images, the longest dimension (34 to 35 mm) of the implant was distorted, and on MRIs, the depth of the implant was affected (1 to 5 mm). The middle distance measure (width of the implant, 22 to 23 mm) was distorted by both imaging techniques. The explanation for these distortions (underestimations) can be attributed to the known directional inaccuracy associated with the imaging of very-low-density/intensity materials caused by the partial volume averaging effect between voxels. Similar (but overestimated) results are typically observed with measurements of very high density/intensity materials, such as titanium mesh, which additionally produces metal artifacts in its vicinity. On the other hand, a sufficient level of accuracy during the manual measurement of the implant cannot be excluded as a confounding variable.

Linear regression analysis showed that cohesion of measures observed in real implant subjects disappears as the image of the implant is observed. In the patient, the MRI showed the UHMW-PE clearly by means of lines and areas with no signal intensity. Therefore, it was possible to recognize its location, adaptation to the bone surface, separation of the orbit from sinuses, and form/shape of the implant, with no significant artifacts; this outcome corresponds to the known results of imaging of other alloplastic materials.[2,9,11–14] On the other hand, a very similar signal pattern is characteristic of gas (ie, air bubbles after injury or surgery) and for the solid bony cortex, so the recognition of UHMW-PE will rely mostly on the subjective experience of the observer.

The surrounding intraorbital soft tissues could also be satisfactorily evaluated. The MRI views allowed visualization of the soft tissues in the region of surgery, especially the muscles. This highlights the superiority of UHMW-PE in MRI to a titanium mesh, which would cause metallic artifacts in its vicinity.

ACKNOWLEDGMENTS

Support for this study was received from the Medical University of Lodz (grant 503/5-061-02/503-01). The authors reported no conflicts of interest related to this study.

REFERENCES

1. Kozakiewicz M, Elgalal M, Walkowiak B, Stefanczyk L. Technical concept of patient-specific, ultrahigh molecular weight polyethylene, orbital wall implant. J Craniomaxillofac Surg 2013;41:282–290.
2. Kozakiewicz M, Elgalal M, Loba P, et al. Clinical application of 3D pre-bent titanium implants for orbital floor fractures. J Craniomaxillofac Surg 2009;37:229–234.
3. Kozakiewicz M, Elgalal M, Loba P, Broniarczyk-Loba A, Stefanczyk L. Treatment with individual orbital wall implants in human – One year ophthalmological observation. J Craniomaxillofac Surg 2011; 39:30–36.
4. Aitasalo K, Kinnunen I, Palmgren J, Varpula M. Repair of orbital floor fractures with bioactive glass implants. J Oral Maxillofac Surg 2001;59:1390–1396.
5. Kontio R, Suuronen R, Salonen O, Paukku P, Konttinen YT, Lindqvist C. Effectiveness of operative treatment of internal orbital wall fracture with polydioxanone implant. J Oral Maxillofac Surg 2001;30:278–285.
6. De Rosa V, Ionna F, Mozzillo N, Parascandolo S, Ziviello M. Tomografia computerizzata spirale con elaborazioni tridimensionali di superficienel trattamento ricostruttivo dei tumori maligni del massiccio facciale. Radiol Med 2000;100:424–428.
7. Olszycki M, Kozakiewicz M, Arkuszewski P, Grzelak P, Stefanczyk L. CT and MRI post-processing reconstructions in maxillo-facial trauma. Pol J Radiol 2004;69:94–99.
8. Weil D, Colangelo L, Badoza D, Zárate J. Alloplastic prosthesis in orbital floor fractures. Ann Ottalmolog Clin Ocul 1996;122:69–76.
9. Cordewener FW, Bos RR, Rozema FR, Houtman WA. Poly(L-lactide) implants for repair of human orbital floor defects: Clinical and magnetic resonance imaging evaluation of long-term results. J Oral Maxillofac Surg 1996;54:9–13.
10. Lattanzi JP, Fein DA, McNeeley SW, Shaer AH, Movsas B, Hanks GE. Computed tomography-magnetic resonance image fusion: A clinical evaluation of an innovative approach for improved tumor localization in primary central nervous system lesions. Radiat Oncol Investig 1997;5:195–205.
11. Park HS, Kim YK, Yoon CJ. Various applications of titanium mesh screen implant to orbital wall fractures. Craniofac Surg 2001;12: 555–560.
12. Sullivan PK, Smith JF, Rozzelle AA. Cranio-orbital reconstruction: Safety and image quality of metallic implants on CT and MRI scanning. Plast Reconstr Surg 1994;94:589–596.
13. Balasundaram I, Al-Hadad I, Parmar S. Recent advances in reconstructive oral and maxillofacial surgery. Br J Oral Maxillofac Surg 2012;50:695–705.
14. Özyuvaci H, Aktas I, Yerit K, Aydin K, Firatli E. Radiological evaluation of sinus lift operation: What the general radiologist needs to know. Dentomaxillofac Radiol 2005;34:199–204.